JACS
JOURNAL OF THE AMERICAN CHEMICAL SOCIETY
Article
pubs.acs.org/JACS

Design of a Metal–Organic Framework with Enhanced Back Bonding for Separation of N_2 and CH_4

Kyuho Lee,[†,‡,§,◆] William C. Isley, III,[‡,∥,◆] Allison L. Dzubak,[‡,∥,◆] Pragya Verma,[‡,∥,◆] Samuel J. Stoneburner,[‡,∥] Li-Chiang Lin,[†,‡] Joshua D. Howe,[†,‡,§] Eric D. Bloch,[‡,⊥] Douglas A. Reed,[⊥] Matthew R. Hudson,[#] Craig M. Brown,[#,▽] Jeffrey R. Long,*[,‡,⊥,○] Jeffrey B. Neaton,*[,‡,§,○] Berend Smit,*[,†,‡,⊥,○] Christopher J. Cramer,*[,‡,∥] Donald G. Truhlar,*[,‡,∥] and Laura Gagliardi*[,‡,∥]

[†]Department of Chemical and Biomolecular Engineering, University of California, Berkeley, California 94720-1462, United States
[‡]Nanoporous Materials Genome Center, University of Minnesota, 207 Pleasant Street Southeast, Minneapolis, Minnesota 55455-0431, United States
[§]Molecular Foundry, Lawrence Berkeley Laboratory, Berkeley, California 94720, United States
[∥]Department of Chemistry, Chemical Theory Center, and Supercomputing Institute, University of Minnesota, Minneapolis, Minnesota 55455-0431, United States
[⊥]Department of Chemistry, University of California, Berkeley, California 94720-1460, United States
[#]Center for Neutron Research, National Institute of Standards and Technology, Gaithersburg, Maryland 20899, United States
[▽]Department of Chemical Engineering, University of Delaware, Newark, Delaware 19716, United States
[○]Materials Sciences Division, Lawrence Berkeley Laboratory, Berkeley, California 94720, United States

Supporting Information

ABSTRACT: Gas separations with porous materials are economically important and provide a unique challenge to fundamental materials design, as adsorbent properties can be altered to achieve selective gas adsorption. Metal–organic frameworks represent a rapidly expanding new class of porous adsorbents with a large range of possibilities for designing materials with desired functionalities. Given the large number of possible framework structures, quantum mechanical computations can provide useful guidance in prioritizing the synthesis of the most useful materials for a given application. Here, we show that such calculations can predict a new metal–organic framework of potential utility for separation of dinitrogen from methane, a particularly challenging separation of critical value for utilizing natural gas. An open V(II) site incorporated into a metal–organic framework can provide a material with a considerably higher enthalpy of adsorption for dinitrogen than for methane, based on strong selective back bonding with the former but not the latter.

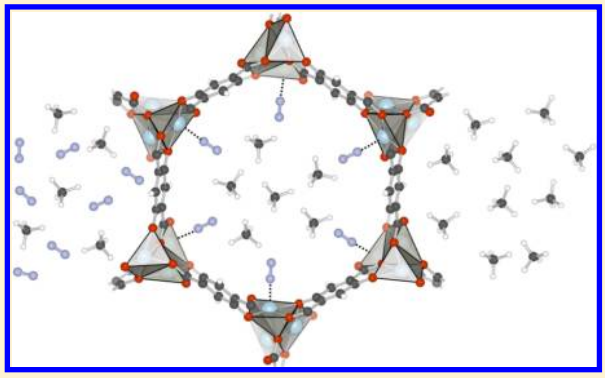

INTRODUCTION

Coordination of dinitrogen to transition-metal cations is important both fundamentally and industrially. Dinitrogen is highly inert and generally considered to be a poor ligand. In 1965, however, it was shown that a simple coordination complex, $[Ru(NH_3)_5]^{2+}$, could reversibly bind N_2.[1] In subsequent years, a number of dinitrogen–transition-metal complexes have been isolated for metals in varying oxidation states with various coordination numbers.[2,3] These complexes typically feature low-valent, relatively reducing metal cations coordinated to dinitrogen in an end-on binding mode. Activating dinitrogen at a metal center to promote its reduction by hydrogen to ammonia under moderate conditions remains a critical goal for homogeneous catalysis. Somewhat weaker metal–dinitrogen binding, however, may be useful for adsorptive separation of gas mixtures. An example is provided by the need to remove dinitrogen (an omnipresent but noncombustible contaminant) from natural gas or other methane-rich gases. This is an extraordinarily difficult separation based on physical properties alone, as both gases lack a permanent dipole and have similar polarizabilities, boiling points, and kinetic diameters. Although cryogenic distillation is currently utilized for separation of these gases, the cost- and capital-intensive nature of this separation has led to development of a number of competing processes, such as membrane- or kinetics-based separations, which generally suffer from low selectivities.[4]

Received: October 8, 2013
Published: December 7, 2013

   dx.doi.org/10.1021/ja4102979 | J. Am. Chem. Soc. 2014, 136, 698–704

Adsorptive separations utilizing porous solids containing transition-metal cations capable of reversibly binding dinitrogen may result in highly selective and efficient dinitrogen/methane separations. Metal−organic frameworks are particularly promising in this regard, as they offer a myriad of materials design opportunities and have already shown great potential for a number of gas separation applications.[5,6] These materials typically display high internal surface areas that can be decorated with both ligand- and metal-based functionalities.[7] In principle, this permits rational design of local environments tuned for selective binding of specific gases. The M-MOF-74 series of compounds having formula M_2(dobdc) (where dobdc^{4-} is 2,5-dioxido-1,4-benzenedicarboxylate) is an especially versatile and intensively studied structure type.[8−13] This structure features 12 Å wide hexagonal channels, lined at the vertices with helical chains of five-coordinate divalent metal ions connected through dobdc^{4-} bridging ligands. Upon activation, these materials have an extremely high density of open metal coordination sites, leading to the possibility of a high working capacity for storage or separation applications.

M-MOF-74 structures containing Mg^{2+}, Mn^{2+}, Fe^{2+}, Co^{2+}, Ni^{2+}, Cu^{2+}, and Zn^{2+} have been synthesized. CH_4 and N_2 adsorption enthalpies reported for a number of these materials indicate they are likely not useful dinitrogen/methane separation materials. For example, Mg-MOF-74 has CH_4 and N_2 adsorption enthalpies of 4.4[14] and 5.0[15] kcal/mol, respectively. However, in principle, other dicationic metals could be incorporated into this structure type. As the synthesis of pure M-MOF-74 phases is often quite challenging, it would be advantageous to know a priori which variations are the best candidates for a given gas separation application. This is a predictive challenge appropriate for application of computational quantum chemistry, which can be used to pinpoint which cations might be anticipated to have interactions of significantly different strengths with competing guests. Interactions between M-MOF-74, corresponding to different M, and various adsorbates were investigated theoretically, which suggested that V-MOF-74 could be promising in N_2/CH_4 separation. We thus decided to study V-MOF-74 in detail. Here, we show, based on three models (Figure 1a−c) of the MOF, that selective back-bonding interactions[16,17] from the vanadium(II) cation centers in V−MOF-74 to the unoccupied π^* orbitals of N_2 can be used to separate N_2/CH_4 mixtures. We further use calculations by Kohn−Sham density functional theory[18] (DFT) and correlated wave function theory (WFT) to put this prediction on a quantitative basis and compare it with the experimentally characterized Fe-MOF-74.

THEORETICAL METHODS

In order to treat the adsorption process reliably, we need to use electronic structure methods that include dynamical correlation, especially attractive medium-range noncovalent forces. Most exchange-correlation (xc) functionals currently used in DFT do not treat such medium-range correlation energy accurately; however, here we use two kinds of density functionals that overcome this limitation. (1) The Rutgers−Chalmers van der Waals density functionals[19] use a nonlocal formulation of the correlation part of the xc functional and can treat attractive van der Waals interactions at both medium range and long range. We use the vdW-DF2+U functional[20] of this type with Hubbard U corrections,[21] where U is a parameter for metal d electrons that is determined to reproduce oxidation energies. (2) The Minnesota functionals[22] include the local kinetic energy density in the xc functional and have been shown to yield accurate noncovalent attraction at van der Waals distances;[23] we will employ three such

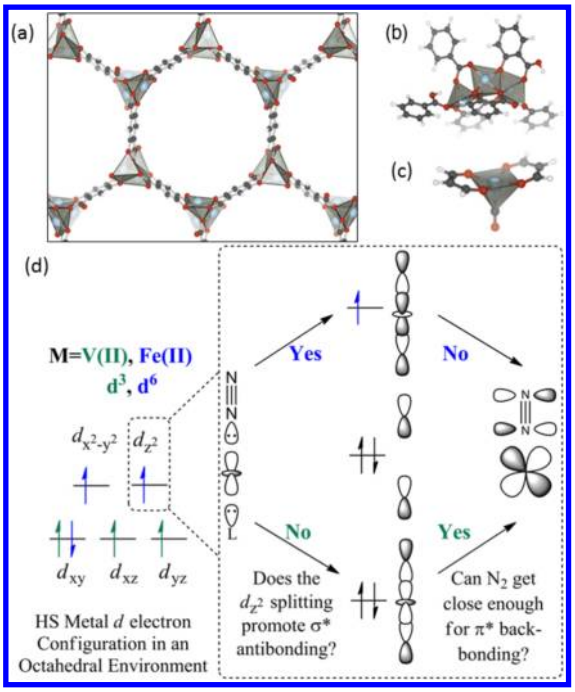

Figure 1. (a−c) Structural models used in this work. (a) Optimized periodic framework model, based on the symmetry of the experimental primitive cell. (b) Eighty-eight-atom cluster. (c) Small model. Light blue, red, dark gray, and white spheres represent vanadium, oxygen, carbon, and hydrogen atoms, respectively. (d) Three-center bonding diagram between framework O atoms, the metal, and a guest. On the left we show the d subshell occupancy of Fe(II) in both blue and green; V(II) would have only three electrons (green alone) in the d subshell, and the metal d_{z^2} orbital would be empty. On the right, the middle section shows how the d_{z^2} orbital splits upon interacting with the four lone pair electrons of two axial Lewis bases; occupancies shown are for Fe(II)—only four electrons would be present for V(II) because the d_{z^2} orbital of V(II) is unoccupied. The right-most orbital diagram shows the nature of the interaction of the ligand-unoccupied π^* orbitals with the occupied $d\pi$ orbitals of the metal; when the antibonding orbital is occupied, the ligand cannot approach the metal as closely, and this interaction is substantially weaker.

functionals, M06-L,[24] M06,[25] and M11-L,[26] because they are based on very different approaches: M06-L is a well-validated[22,23,25] local functional with global parameters, M11-L is a recent local functional employing different exchange and correlation parameters for short and long interelectronic distances, and M06 employs 27% Hartree−Fock exchange, as justified by adiabatic connection arguments[27] to reduce DFT self-interaction error.

We also employ two WFT methods, in particular, local-pair natural-orbital coupled cluster theory with single and double excitations[28] (LPNO-CCSD) and complete active space second-order perturbation theory with counterpoise corrections (CASPT2-CP).[29] The latter method has been shown to yield accurate energetics in systems containing transition-metal compounds.[30,31]

The DFT and WFT methods used here involve approximations that impose limits on their accuracy. Because they represent very different approaches to the electronic structure problem, confidence in the utility of their quantitative predictions is significantly increased when different models agree, even if the natures of the various approximations employed make it unclear which model is most accurate within the remaining variation.

Orbitals, Spin States, Cores, Relativistic Effects, and Metal Ions. In Kohn−Sham calculations and in the reference state for LPNO-CCSD, the V and Fe ions are in high-spin states (quartet and quintet, respectively) and all other orbitals are doubly occupied. For the CASPT2-CP calculation on the 88-atom cluster, we replace the

dx.doi.org/10.1021/ja4102979 | J. Am. Chem. Soc. 2014, 136, 698−704

two outer metal ions by closed-shell Zn(II) ions and treat the central metal in the active space. (None of the DFT calculations involve this Zn substitution.) Descriptions of the active spaces used for all species are given in the Supporting Information. The vdW-DF2 calculations with the Hubbard U correction employ the all-electron projector-augmented wave (PAW) method for scalar relativistic core electrons and ionic potentials; all other calculations treat all electrons explicitly. CASPT2-CP calculations use the Douglas−Kroll−Hess relativistic approximation, and the extended transition state (ETS) method for energy decomposition analysis combined with the natural orbitals for chemical valence (NOCV) theory calculations use the ZORA relativistic approximation. All other calculations are nonrelativistic.

Basis Sets. All vdW-DF2+U calculations employed a plane-wave basis with a 1000 eV kinetic energy cutoff. All other DFT calculations employed the def2-TZVP basis except the ETS-NOCV analysis, which used TZ2P. LPNO-CCSD calculations are extrapolated to a complete basis set from def2-TZVP and def2-QZVP. CASPT2-CP calculations for the small model employed the ANO-RCC-TZVP basis for all atoms, and for the 88-atom cluster they employed the ANO-RCC-DZVP basis for all atoms. References for basis sets are in Supporting Information.

Coordinates. We used a triclinic primitive unit cell containing 54 atoms including 6 metal centers and simultaneously optimized the lattice vectors and atomic positions in the unit cell with variable cell dynamics with PBE+U for bare MOFs and with vdW-DF2+U for adsorbates. The 88-atom clusters were taken out of these periodic structures. Optimization of binding geometry of adsorbates in the periodic MOFs and on the 88-atom cluster involved freezing the MOF and optimizing only the coordinates of the adsorbate; this was carried out with all DFT calculations. The structure of the small model was fully optimized by M06-L, and these structures were used for the LPNO-CCSD and CASPT2-CP calculations. Full coordinates and absolute energies in hartrees of selected structures are in the Supporting Information.

Starting geometries for the periodic model were based on the experimental structures[8−10,12,32] of M-MOF-74 (Figure 1a) and further optimized by DFT; the primitive unit cell of experimental structure contains 54 atoms, including 6 metal centers. We defined two other models of M-MOF-74 to be studied at additional levels of theory. The cluster (Figure 1b) has 88 atoms, including three metal centers, and it was designed[13] to retain the local structure of MOF-74 about the central metal ion while remaining small enough for high-level electronic structure calculations. The small model (Figure 1c) has 19 atoms, including one metal center, and is small enough to conduct calculations by expensive wave function methods for comparison.

All iron and vanadium ions were modeled in their respective ground (high-spin) state. To maintain charge neutrality with all oxide ligands in the small model, we included a trans carbonyl ligand. Although carbonyl groups are usually considered to be strong-field ligands, the small model nevertheless maintains a high-spin ground state and an electronic structure consistent with the larger model. Indeed, the insensitivity of our conclusions to the nature of the trans ligand in the M-MOF-74 model provides particularly strong support for our analysis.

Charges. Partial atomic charges were calculated by charge model 5 (CM5).[33,34]

Software. Minnesota functionals, Gaussian 09;[35,36] vdW-DF2+U, VASP;[37] LPNO-CCSD, ORCA 2.9.1;[38] CASPT2-CP, Molcas 7.8;[39] ETS-NOCV, ADF.[40−42]

RESULTS AND DISCUSSION

N_2 bonding motif to V-MOF-74 and Fe-MOF-74. A molecular orbital picture can be used to predict selective adsorption of N_2 over CH_4 with V-MOF-74. The model exploits the square-pyramidal coordination geometry of the metal in desolvated M-MOF-74 (Figure 1d). A key consideration is the d^3 electronic configuration of V(II). In the case of N_2 binding, our DFT calculations show that a three-center bond is formed between the framework oxo ligand trans to dinitrogen, the metal, and N_2 (Figure 1d). Given an end-on coordination geometry, a pair of nonbonding electrons on N_2 and its respective trans framework atom interact with the V(II) d_{z^2} orbital, and the net result is a three-center bond with two electrons each in a bonding and nonbonding orbital. In addition to the resulting σ bond, the unoccupied π^* orbitals of N_2 can accept back-bonding electrons from the metal $d\pi$ orbitals. This back bonding is *not* present for methane, due to the lack of low-energy π^* orbitals on the hydrocarbon. Fe(II), in contrast, has a high-spin d^6 electronic configuration with a singly occupied d_{z^2} orbital. In this case, the two doubly occupied lone pairs provide four electrons to the three-center bond and the occupation of the metal d_{z^2} orbital provides one electron, for a total of five electrons in the three-center bond; so, one electron is in the antibonding orbital. As the N_2 approaches the metal site, it thus experiences unfavorable σ antibonding plus additional exchange repulsion from the occupied nonbonding orbital. Consequently, N_2 cannot approach the Fe(II) center closely enough to experience π^* back-bonding stabilization as favorable as is present in the V(II)−N_2 system.

In subsequent sections of this article, we confirm the differential stabilization effect with local and nonlocal DFT calculations, confirming our molecular orbital prediction that as-yet unsynthesized V-MOF-74 could be used to separate N_2 from CH_4. We also reinforce our DFT results with correlated wave function calculations to rule out the possibility of artificial back bonding[43] owing to the possible underestimation of the energy gap and the delocalization of d electrons in the DFT models. Finally, we analyze single-determinantal Kohn−Sham reference functions to confirm the above explanation of the effect.

N_2 and CH_4 Adsorption in V-MOF-74 and Fe-MOF-74. The key quantity we calculated is the differential adsorption energy defined by

$$\Delta E_{ads} = E_{ads}(N_2) - E_{ads}(CH_4)$$

where E_{ads} is the energy of adsorption (here defined as a positive number to denote that deadsorption is endoergic); thus, ΔE_{ads} is more positive when N_2 binds more strongly. The results are in Table 1. Across all levels of theory and all models, CH_4 binding is comparable between the two metals but N_2 is predicted to bind significantly more strongly than CH_4 to the coordinatively unsaturated metal site when the metal is V rather than Fe.

We noted above the consistent trend observed for calculated ΔE_{ads} values; the trends in calculated E_{ads} values are also

Table 1. N_2/CH_4 Adsorption Energy Differences, ΔE_{ads} (in kcal/mol)

	small model		large models[a]	
level of theory	V	Fe	V	Fe
DFT, vdW-DF2+U			6.0	0.4
DFT, vdW-DF2+U	4.9	0.4	5.8	0.3
DFT, M06-L	4.3	0.0	10.1	0.9
DFT, M06	4.5	0.1	6.9	0.4
DFT, M11-L	4.2	−0.8	5.9	−1.7
DFT, LPNO-CCSD/CBS	4.8	0.7	*b*	*b*
WFT, CASPT2 CP	3.8	0.3	2.1	0.3

[a]The first row is for the periodic model, and the other large-model calculations are for the 88-atom cluster. [b]Impractically computationally intensive.

dx.doi.org/10.1021/ja4102979 | J. Am. Chem. Soc. 2014, 136, 698−704

consistent across the methods. Absolute adsorption energies for the 88-atom cluster and the periodic model are compared in Table 2. We see remarkable agreement between the adsorption

Table 2. Absolute Binding Energies (kcal/mol)

	V−N_2	Fe−N_2	V−CH_4	Fe−CH_4
periodic model				
vdW-DF2+U	13.4	6.6	7.4	6.3
88-atom cluster				
vdW-DF2+U	12.0	4.5	6.2	4.2
M06-L	19.9	7.8	9.8	6.9
M06	17.5	8.1	10.6	7.7
M11-L	13.4	4.4	7.5	6.1
CASPT2 CP	7.4	3.3	5.3	3.0
small model				
vdW-DF2+U	8.5	3.2	3.6	2.9
M06-L	9.1	4.3	4.8	4.3
LPNO-CCSD/CBS	9.6	4.2	4.8	3.6
CASPT2 CP	6.5	3.3	2.7	3.0

energies calculated with the 88-atom cluster and the periodic model and further remarkable agreement between the absolute binding energies calculated by DFT with different functionals and by WFT; the good agreement of results obtained with several methods that incorporate the physics in different ways adds confidence to the predictions. Inspection of Table 2 shows relatively large differences in the absolute binding energies between the large and small clusters. The enhanced attraction in the 88-atom cluster model can partially be attributed to greater medium-range correlation effects. One should also consider that the two models have different ligand coordination environments, and this too has an influence on the absolute binding energies.

In order to further verify the validity of these predictions, isosteric heats of CH_4 and N_2 adsorption in Fe_2(dobdc) were obtained experimentally from adsorption isotherms at 175 K. (Details of the experiment are in the Supporting Information.) As seen in Figure 2, the uptake of N_2 in Fe-MOF-74 is relatively steep and approaches one N_2 molecule per iron cation site at 1 bar and 175 K. Methane uptake, while similar at low pressure, reaches a higher value of approximately 1.5 CH_4 molecules per iron at 1 bar. These plots yield isosteric heats of adsorption for methane and dinitrogen that are both relatively low and quite similar; in particular, they are 5.3 ± 0.2 and 5.5 ± 0.2 kcal/mol, respectively, which yields an experimental difference of 0.2 ± 0.3 kcal/mol. These results differ from the previously reported values of 4.8 kcal/mol for CH_4[44] and 8.4 kcal/mol for N_2[12] both because of the lower temperature and because of the change in experimental procedure; the present results should be more accurate for the difference because they were done with isotherms at the same temperature on the exact same batch of sample. An attempt to obtain the same information for V-MOF-74 was not successful.

Experimental *enthalpies* of adsorption should not be compared directly to the *energies* of adsorption in Table 2. For the 88-atom cluster, however, we computed the enthalpies of adsorption at 175 K by a formula given previously.[13] The M06-L, M06, and M11-L levels of theory give predicted differences in adsorption enthalpy of 1.1, 0.5, and −1.6 kcal/mol, respectively. The average difference in predicted adsorption enthalpy of 0.0 kcal/mol is in good agreement with the 0.2 kcal/mol difference observed experimentally.

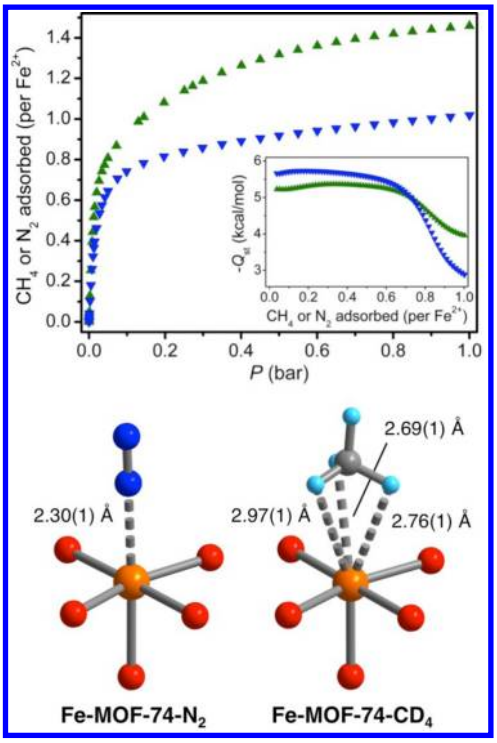

Figure 2. (Top) Adsorption of methane (green) and dinitrogen (blue) in Fe_2(dobdc) at 175 K. (Top inset) Isosteric heats of adsorption. (Bottom) First coordination spheres for the iron centers in the solid-state structures obtained upon dosing Fe-MOF-74 with dinitrogen or methane; orange, red, blue, gray, and light blue represent iron, oxygen, nitrogen, carbon, and deuterium, respectively.

Structural Parameters, Vibrational Frequencies, and Charges. Table 3 shows that the M−N distance is shorter in

Table 3. M06-L Bond Distances, Adsorbate Frequencies, and Partial Atomic Charges

		small model		88-atom cluster	
	gas phase	V	Fe	V	Fe
structural descriptors: binding N_2					
M−N (Å)		2.21	2.73	2.08	2.34
ν_{N-N} (cm^{-1})	2424	2357	2430	2252	2360
structural descriptors: binding CH_4					
M−C (Å)		3.00	3.15	2.77	2.96
ν_{C-H} (cm^{-1})	3057	3037	3043	3017	3031
partial atomic charges: bare MOF					
M		0.90	0.69	0.81	0.69
partial atomic charges: binding N_2					
M		0.89	0.66	0.88	0.70
N_2	0.00	0.01	0.07	−0.09	0.09
partial atomic charges: binding CH_4					
M		0.85	0.66	0.74	0.66
CH_4	0.00	0.06	0.03	0.05	0.08

V-MOF-74 than in Fe-MOF-74, as anticipated above; there is also a smaller difference in the M−C distances for CH_4. Neutron powder diffraction experiments on Fe-MOF-74 at 10 K (see figure in the Supporting Information) indicate excellent agreement between the calculated and the experimentally observed structures of methane bound to Fe^{2+}. Specifically, the Fe−C distance of 2.98(1) Å is very close to the distance of 2.96 Å calculated for the 88-atom cluster. Differences in M−N

dx.doi.org/10.1021/ja4102979 | J. Am. Chem. Soc. 2014, 136, 698−704

distances are consistent with the energetic results presented above.

The potential energy curves (given in Figure 3) provide further evidence for qualitatively different kinds of interaction;

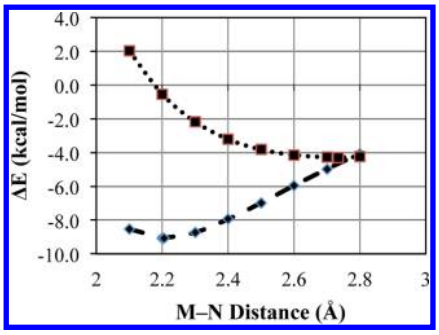

Figure 3. Potential energy curve as a function of M−N_2 distance for the small model as calculated with the M06-L exchange−correlation functional. The curve for M = V(II) is shown as a dashed line with diamond points indicating single-point energies. The curve for M = Fe(II) is shown as a dotted line with square points indicating single-point energies.

we give just one example, the interaction of N_2 with M in the small model, calculated by M06-L. Single-point energies were calculated by modifying the M−N_2 distance but keeping all other geometrical parameters unchanged from the geometric minima. Interestingly, the predicted interaction energy at 2.8 Å is nearly equivalent for N_2 with the Fe and V small models. At an M−N distance of 2.8 Å, the interaction energy is ∼−4 kcal/mol for both V and Fe. As N_2 approaches more closely, the potential energy reaches a minimum of −4.3 kcal/mol at 2.73 Å for Fe but goes to a much deeper well at −9.1 kcal/mol at 2.21 Å for V. (This further reinforces the conclusion that the binding interaction to vanadium is quite different from that of other metals studied.) For comparison, the Fe−N distance was determined to be 2.30±0.01 Å for N_2 adsorbed within Fe-MOF-74 by neutron diffraction experiments at 9 K. The predicted Fe−N distance for the 88-atom cluster compares favorably with the measured value of 2.30±0.01 Å.

The N−N stretching frequency is a probe of back bonding, because these shifts result from weakening the bond by d$\pi \rightarrow \pi^*$ back-donation. Periodic vdW-DF2+U calculations show that, as compared to the isolated gas-phase diatomic vibrational frequency (2415 cm^{-1}), N_2 bound to V experiences a significant shift in the N−N stretch (−102 cm^{-1}), whereas N_2 bound to Fe shows a negligible change (−6 cm^{-1}). In contrast, vibrational frequency shifts for C−H modes in CH_4, where no back bonding is predicted, are negligible. For the 88-atom cluster, M06 calculations for N_2 bound to MOF show similar trends—a 103 cm^{-1} shift for V and a 4 cm^{-1} shift for Fe. M11-L also shows similar shifts: 101 and 5, respectively. Table 3 shows a more complete set of results for M06-L, and these too are consistent with our analysis.

Next we examine in more detail the amount of charge transfer between the metal and the N_2 guest. Key charges in atomic units are given in Table 3.

The total charge on the guest molecule is computed by summing the partial charges of the individual atoms of the guest molecule; this indicates the magnitude and direction of charge transfer between the MOF and the guest. For each of the three functionals, CM5 partial atomic charges for the 88-atom cluster indicate donation of negative charge from the central metal ion to the nitrogen molecule and an opposite direction of transfer for methane. This is also reflected in the charge on the metal ion being increased for N_2 adsorption and decreased for CH_4 adsorption when compared to the bare MOF. The increase or decrease in the positive charge of the central metal ion with N_2/CH_4 adsorption does not exactly equal the total charge on the guest molecule. This reflects charge change within the rest of the MOF framework.

We find that the direction of electron transfer from the metal center to the guest molecule for the Fe−N_2 system is *opposite* to what is observed for V−N_2. Specifically, the partial atomic charge on Fe is 0.66 in the presence of either N_2 or CH_4; these values are the same as the values of 0.66 for the bare Fe-MOF-74 framework. The partial atomic charge on the V ions in V-MOF-74 is significantly higher in all structures, and it is not very sensitive to the adsorbates in the small model, but in the 88-atom cluster the partial atomic charge on V increases by 0.07 upon adsorption of N_2 and decreases by 0.07 upon adsorption of CH_4. Overall, these changes are consistent with our interpretation of increased back bonding in the V−N_2 case.

Orbital Analysis. The nature of the M−N_2 bond of the small model was investigated using the extended transition state (ETS) method for energy decomposition analysis combined with the natural orbitals for chemical valence (NOCV) theory. ETS-NOCV analysis[45] separates bond formation energy into distortion of interacting subsystems, steric interaction (with electrostatic and exchange-correlation contributions), and an "orbital" term that represents a combination of the interactions between the occupied molecular orbitals on one bonding partner with the unoccupied molecular orbitals of the other and the intrafragment polarization. ETS-NOCV calculations carried out on the small model with M06-L show (see Figure 4) that both σ donation and π^* back-bonding interactions are weaker

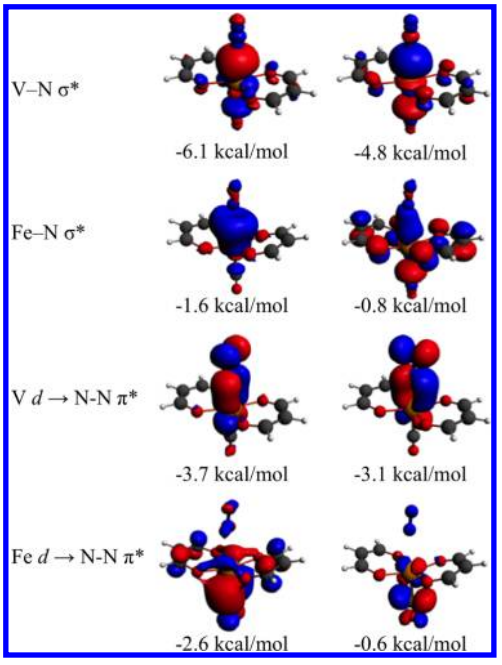

Figure 4. Contours of NOCVs for N_2 binding with V-MOF-74 and Fe-MOF-74. Four NOCV orbitals with the largest contributions to the binding enrgy are reported for each case, with the sum of the α and β spin contributions to the bond energy shown immediately below. Only the positive eigenvalue NOCV's are shown, as the negative eigenvalue NOCV's have similar character.

dx.doi.org/10.1021/ja4102979 | J. Am. Chem. Soc. 2014, 136, 698−704

for Fe−N_2 than for V−N_2. Comparing the two largest alpha and beta spin-paired NOCV contributions to the bond energy, the σ interactions are about eight times stronger for V than for Fe and the π^* back-bonding-type interactions are about twice as strong, with all other contributions being less than 1 kcal/mol for V and less than 0.5 kcal/mol for Fe. Such analyses of charge rearrangement are not unique, so we also performed natural bond order (NBO) analysis,[46] as described next, to test the robustness of this interpretation.

NBO analysis on the small model identifies a σ bond for V−N_2 but not for Fe−N_2. Second-order perturbation analysis of the Kohn−Sham matrix in the NBO basis shows that back bonding, defined as the interaction between occupied π-type NBO orbitals and unoccupied π^*-type NBO orbitals of N_2, is stronger for V than for Fe. Summing the contribution from orbitals with occupations greater than 0.8 electrons, the total back-bonding interaction is 32 kcal/mol for V−N_2 and 13 kcal/mol for Fe−N_2.

Given its predicted N_2/CH_4 separation capabilities rationalized above, we initiated efforts to synthesize V-MOF-74. To date, isolation of crystalline material, rather than amorphous powders (as determined by powder X-ray diffraction), has proven elusive, highlighting another MOF challenge: the need for a greater understanding of the mechanisms by which metal−organic frameworks form. The present computational results strongly motivate continued efforts to realize both of these goals.

CONCLUSIONS

We predict that dinitrogen separation from methane can be accomplished by the as-yet-unsynthesized V-MOF-74, because the vanadium ions in this MOF have their interaction energies significantly increased by π back bonding with N_2 but not with CH_4. This provides a new M-MOF-74 target as a challenge to synthesis. Our qualitative analysis is placed on a quantitative footing by a variety of density functional and wave function calculations of relative binding energies using models validated against experimental binding energies for the analogous Fe-MOF-74. Density functional calculations are also analyzed to provide detailed insights into bonding distances, charge transfer, vibrational frequency shifts, and orbital interactions.

ASSOCIATED CONTENT

Supporting Information

More details about the calculations, references for basis sets, powder diffraction experimental data, and gas adsorption measurements. This material is available free of charge via the Internet at http://pubs.acs.org.

AUTHOR INFORMATION

Corresponding Authors

jrlong@berkeley.edu
jbneaton@lbl.gov
berend-smit@berkeley.edu
cramer@umn.edu
truhlar@umn.edu
gagliard@umn.edu

Author Contributions

◆These authors (K.L., W.C.I., A.L.D., and P.V.) contributed equally.

Notes

The authors declare no competing financial interest.

ACKNOWLEDGMENTS

We gratefully acknowledge Xuefei Xu, Joshua Borycz, Rémi Maurice, Robert Berger, Roberta Poloni, James Phillips, and Pere Miró for helpful discussions. This research was supported by the U.S. Department of Energy, Office of Basic Energy Sciences, Division of Chemical Sciences, Geosciences, and Biosciences under award DE-FG02-12ER16362. Portions of this work were performed at the Molecular Foundry, supported by the Office of Science, Office of Basic Energy Sciences, of the U.S. Department of Energy under Contract No. DEAC02-05CH11231. Portions of the computations were performed using NERSC. W.C.I. is grateful for a Kenneth E. and Marion S. Owens Endowed Fellowship. A.L.D. is grateful for support through the Louise T. Dosdall Fellowship. M.R.H. acknowledges the NIST NRC Postdoctoral Fellowship research program for support. E.D.B. was supported by a Gerald K. Branch fellowship in chemistry. P.V. acknowledges a Phillips 66 Departmental Excellence Fellowship.

REFERENCES

(1) Allen, A. D.; Senoff, C. V. *J. Chem. Soc., Chem. Commun.* **1965**, *24*, 621.
(2) Fryzuk, M. D.; Johnson, S. A. *Coord. Chem. Rev.* **2000**, *200−202*, 379.
(3) Allen, A. D.; Harris, R. O.; Loescher, B. R.; Stevens, J. R.; Whiteley, R. N. *Chem. Rev.* **1973**, *73*, 11.
(4) Lokhandwala, K. A.; Pinnau, I.; He, Z.; Amo, K. D.; DaCosta, A. R.; Wijmans, J. G.; Baker, R. W. *J. Membr. Sci.* **2010**, *346*, 270.
(5) Duren, T.; Bae, Y. S.; Snurr, R. Q. *Chem. Soc. Rev.* **2009**, *38*, 1237.
(6) Li, J. R.; Kuppler, R. J.; Zhou, H. C. *Chem. Soc. Rev.* **2009**, *38*, 1477.
(7) McDonald, T. M.; Lee, W. R.; Mason, J. A.; Wiers, B. M.; Hong, C. S.; Long, J. R. *J. Am. Chem. Soc.* **2012**, *134*, 7056.
(8) Rosi, N. L.; Kim, J.; Eddaoudi, M.; Chen, B.; O'Keeffe, M.; Yaghi, O. M. *J. Am. Chem. Soc.* **2005**, *127*, 1504.
(9) Dietzel, P. D. C.; Morita, Y.; Blom, R.; Fjellvag, H. *Angew. Chem., Int. Ed.* **2005**, *44*, 6354.
(10) Dietzel, P. D. C.; Panella, B.; Hirscher, M.; Blom, R.; Fjellvag, H. *Chem. Commun.* **2006**, 959.
(11) Nijem, N.; Veyan, J. F.; Kong, L.; Li, K.; Pramanik, S.; Zhao, Y.; Li, J.; Langreth, D.; Chabal, Y. J. *J. Am. Chem. Soc.* **2010**, *132*, 1654.
(12) Bloch, E. D.; Murray, L. J.; Queen, W. L.; Chavan, S.; Maximoff, S. N.; Bigi, J. P.; Krishna, R.; Peterson, V. K.; Grandjean, F.; Long, G. J.; Smit, B.; Bordiga, S.; Brown, C. M.; Long, J. R. *J. Am. Chem. Soc.* **2011**, *133*, 14814.
(13) Verma, P.; Xu, X.; Truhlar, D. G. *J. Phys. Chem. C* **2013**, *117*, 12648.
(14) Wu, H.; Zhou, W.; Yildirim, T. *J. Am. Chem. Soc.* **2009**, *131*, 4995.
(15) Valenzano, L.; Civalleri, B.; Chavan, S.; Palomino, G. T.; Arean, C. O.; Bordiga, S. *J. Phys. Chem. C* **2010**, *114*, 11185.
(16) Yamamoto, A. *Organotransition Metal Chemistry*; Wiley: New York, 1986.
(17) Crabtree, R. H. *The Organometallic Chemistry of the Transition Metals*, 2nd ed.; Wiley: New York, 1994.
(18) Kohn, W.; Becke, A. D.; Parr, R. G. *J. Phys. Chem.* **1996**, *100*, 12974.
(19) Dion, M.; Rydberg, H.; Schroder, E.; Langreth, D. C.; Lundqvist, B. I. *Phys. Rev. Lett.* **2004**, *92*, 246401.
(20) Lee, K.; Murray, E. D.; Kong, L.; Lundqvist, B. I.; Langreth, D. C. *Phys. Rev. B.* **2010**, *82*, 081101.
(21) Liechtenstein, A. I.; Anisimov, V. I.; Zaanen, J. *Phys. Rev. B* **1995**, *52*, R5467.
(22) Zhao, Y.; Truhlar, D. G. *Acc. Chem. Res.* **2008**, *41*, 157.
(23) Zhao, Y.; Truhlar, D. G. *Chem. Phys. Lett.* **2011**, *502*, 1.
(24) Zhao, Y.; Truhlar, D. G. *J. Chem. Phys.* **2006**, *125*, 194101.
(25) Zhao, Y.; Truhlar, D. G. *Theor. Chem. Acc.* **2008**, *120*, 215.

(26) Peverati, R.; Truhlar, D. G. *J. Phys. Chem. Lett.* **2012**, *3*, 117.
(27) Becke, A. D. *J. Chem. Phys.* **1993**, *98*, 1372.
(28) Neese, F.; Hansen, A.; Liakos, D. G. *J. Chem. Phys.* **2009**, *131*, 064103.
(29) Andersson, K.; Malmqvist, P. A.; Roos, B. O. *J. Chem. Phys.* **1992**, *96*, 1218.
(30) Fohlmeister, L.; Liu, S.; Schulten, C.; Moubaraki, B.; Stasch, A.; Cashion, J. D.; Murray, K. S.; Gagliardi, L.; Jones, C. *Angew. Chem., Int. Ed.* **2012**, *51*, 8294.
(31) LiManni, G.; Dzubak, A. L.; Mulla, A.; Brogden, D. W.; Berry, J. F.; Gagliardi, L. *Chem.—Eur. J.* **2012**, *18*, 1737.
(32) Sanz, R.; Martinez, F.; Orcajo, G.; Wojtas, L.; Briones, D. *Dalton Trans.* **2013**, *42*, 2392.
(33) Marenich, A. V.; Jerome, S. V.; Cramer, C. J.; Truhlar, D. G. *J. Chem. Theor. Comput.* **2012**, *8*, 527.
(34) Marenich, A. V.; Cramer, C. J.; Truhlar, D. G. *CM5PAC*; University of Minnesota: Minneapolis. 2011.
(35) Frisch, M. J.; et al. *Gaussian 09*, Revision C.01; Gaussian, Inc.: Wallingford, CT, 2010.
(36) Zhao, Y.; Peverati, R.; Yang, K. R.; Truhlar, D. G. *MN-GFM 6.4*; University of Minnesota: Minneapolis, 2012.
(37) Kresse, G.; Furthmuller, J. *Phys. Rev. B* **1996**, *54*, 11169.
(38) Neese, F. *WIREs Comput. Mol. Sci.* **2012**, *2*, 73.
(39) Aquilante, F.; et al. *J. Comput. Chem.* **2010**, *31*, 224.
(40) Baerends, E. J.; et al. *ADF2013, SCM*; Theoretical Chemistry, Vrije Universiteit: Amsterdam, The Netherlands, 2013; http://www.scm.com.
(41) te Velde, G.; Bickelgaupt, F. M.; van Gisbergen, S. J. A.; Fonseca Guerra, C.; Baerends, E. J.; Snijders, J. G.; Ziegler, T. *J. Comput. Chem.* **2001**, *22*, 931.
(42) Fonseca Guerra, C.; Snijders, J. G.; te Velde, G.; Baerends, E. J. *Theor. Chem. Acc.* **1998**, *99*, 391.
(43) Kresse, G.; Gil, A.; Sautet, P. *Phys. Rev. B* **2003**, *68*, 073401.
(44) Bloch, E. D.; Queen, W. L.; Krishna, R.; Zadrozny, J. M.; Brown, C. M.; Long, J. R. *Science* **2012**, *335*, 1606.
(45) Mitoraj, M.; Michalak, A.; Ziegler, T. *J. Chem. Theor. Comput.* **2009**, *5*, 962.
(46) Reed, A. E.; Curtiss, L. A.; Weinhold, F. *Chem. Rev.* **1998**, *88*, 899.